On the Definition of Marginal Ice Zone Width

COURTENAY STRONG

Department of Atmospheric Sciences, University of Utah, Salt Lake City, Utah

DALLAS FOSTER[a] AND ELENA CHERKAEV

Department of Mathematics, University of Utah, Salt Lake City, Utah

IAN EISENMAN

Scripps Institution of Oceanography, University of California, San Diego, La Jolla, California

KENNETH M. GOLDEN

Department of Mathematics, University of Utah, Salt Lake City, Utah

(Manuscript received 4 September 2016, in final form 29 March 2017)

ABSTRACT

Sea ice features a dense inner pack ice zone surrounded by a marginal ice zone (MIZ) in which the sea ice properties are modified by interaction with the ice-free open ocean. The width of the MIZ is a fundamental length scale for polar physical and biological dynamics. Several different criteria for establishing MIZ boundaries have emerged in the literature—wave penetration, floe size, sea ice concentration, etc.—and a variety of definitions for the width between the MIZ boundaries have been published. Here, three desirable mathematical properties for defining MIZ width are proposed: invariance with respect to translation and rotation on the sphere; uniqueness at every point in the MIZ; and generality, including nonconvex shapes. The previously published *streamline* definition is shown to satisfy all three properties, where *width* is defined as the arc length of a streamline through the solution to Laplaces's equation within the MIZ boundaries, while other published definitions each satisfy only one of the desired properties. When defining MIZ spatial average width from streamline results, the rationale for averaging with respect to distance along both MIZ boundaries was left implicit in prior studies. Here it is made rigorous by developing and applying the mathematics of an analytically tractable idealization of MIZ geometry—the eccentric annulus. Finally, satellite-retrieved Arctic sea ice concentrations are used to investigate how well streamline-based MIZ spatial average width is approximated by alternative definitions that lack desirable mathematical properties or local width values but offer computational efficiency.

1. Introduction

Declines in Arctic sea ice coverage, age, and thickness over the past few decades have been dramatic and appear to be accelerating, particularly during the warm season (Polyakov et al. 2012; Comiso 2012; Stammerjohn et al. 2012; Cavalieri and Parkinson 2012, and references therein). Record-breaking extent minima and abrupt changes in Arctic sea ice seasonality have been observed, including an abrupt increase in the amplitude of the seasonal cycle since 2007 (Stammerjohn et al. 2012; Livina and Lenton 2013). These changes in Arctic sea ice suggest scientifically important changes in the position, width, and area of the marginal ice zone (MIZ)—a dynamic and biologically active region that transitions from the dense inner pack ice zone to open ocean (e.g., Squire 1998; Wadhams 2000; Squire 2007; Weeks 2010; Barber et al. 2015). The width of the MIZ in particular is recognized as a fundamental length scale for climate dynamics and polar ecosystem dynamics (e.g., Wadhams 2000; Stroeve et al. 2016). The MIZ represents a region of

[a] Current affiliation: Department of Mathematics, Oregon State University, Corvallis, Oregon.

Corresponding author: Courtenay Strong, court.strong@utah.edu

DOI: 10.1175/JTECH-D-16-0171.1

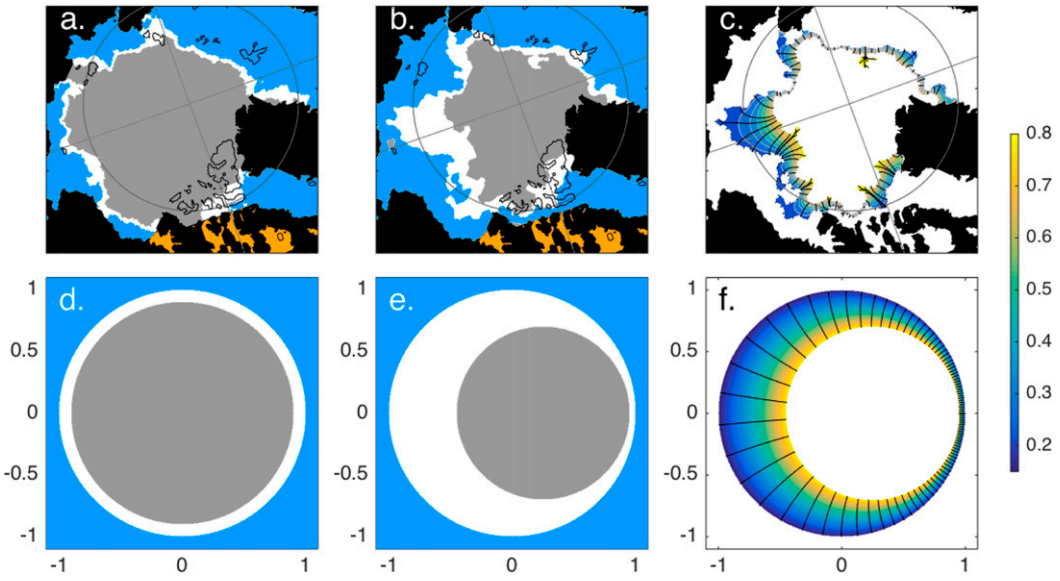

FIG. 1. (a) For 18 Sep 1984, the inner pack ice is shaded gray, the MIZ is shaded white, and sparse ice and open ocean are shaded blue. Land is shaded black, islands over which concentrations were interpolated are outlined in black, and bays or inland seas where the MIZ was not analyzed are shaded orange. (b) As in (a), but for 29 Aug 2010. (c) Solution to Laplace's equation within the MIZ (ϕ) is shaded, and black curves are streamlines through ϕ whose arc length define MIZ width. (d)–(f) How eccentric annulus models can be used to approximate the observed patterns in (a)–(c). Specifically, (d),(e) are eccentric annuli (white shading) that approximate the geometry in (a),(b), respectively. (f) Simplified, eccentric annulus version of (c) constructed by solving Laplace's equation within the MIZ from (e).

intense air–sea ice interactions that have major effects on atmospheric boundary layer structure and meteorological processes (e.g., Shaw et al. 1991; Glendening 1994), and the MIZ provides a physical buffer that largely protects the more consolidated inner pack from the effects of ocean waves (e.g., Squire 2007). Increasing Arctic open water area may allow waves to evolve into swells that enhance sea ice breakup and further accelerate sea ice retreat (Thomson and Rogers 2014). The width of the MIZ and its variability are important drivers of marine habitat selection for a broad range of biota (Ribic et al. 1991; Perrette et al. 2010; Post et al. 2013; Williams et al. 2014), including Antarctic minke whales (Williams et al. 2014). Finally, changes in the MIZ also impact human accessibility to the Arctic, as broken ice in the MIZ is more navigable than dense inner pack ice (Stephenson et al. 2011; Schmale et al. 2013; Rogers et al. 2013).

Strong (2012) introduced an objective and automated method for identifying and measuring the width of the MIZ from satellite-retrieved sea ice concentrations. A follow-up application of the method to satellite data (Strong and Rigor 2013) revealed that the warm-season (July–September) Arctic MIZ widened over the past three decades by 39% while moving poleward and that the cold-season (February–April) Arctic MIZ narrowed by 15% over the same period. A representative warm-season sea ice configuration from early in the satellite record (Fig. 1a) shows a large region of inner pack ice (gray shading) surrounded by a narrow MIZ (white shading). More recently in the satellite era (Fig. 1b), the inner pack ice has retreated more rapidly than the marginal ice, leaving a markedly widened MIZ, particularly in the East Siberian and Beaufort Seas.

There are challenges associated with objective definition and automated analysis of MIZ width in part because of the nonconvex shape of the MIZ (e.g., Fig. 1b). In medical imaging, Jones et al. (2000) introduced a definition of the width of a nonconvex region as the arc length of a curve (streamline) along $\nabla\phi$, where ϕ is the solution of Laplace's equation ($\nabla^2\phi = 0$) in this region. Strong (2012) adapted this definition of width to the MIZ as illustrated in Fig. 1c. In this example, the solution to $\nabla^2\phi = 0$ was obtained numerically with MIZ ice concentration boundary conditions $\phi = 0.80$ on the high-concentration edge adjacent to dense inner pack ice and $\phi = 0.15$ on the low-concentration edge adjacent to open ocean. Strong (2012) defined MIZ width by averaging the arc length of the streamlines with respect to distance along the perimeter of the MIZ, but other definitions are possible (e.g., averaging the arc lengths with respect to area). Stroeve et al. (2016) measured the width of the Antarctic MIZ along meridians, finding that the

significance of trends depended on the algorithm used to retrieve concentration from the passive microwave satellite data.

The motivation of the present study is to provide a mathematically rigorous basis for defining MIZ width and MIZ spatial average width. The first novel component in the manuscript is articulation and illustration of three desirable mathematical properties for width: invariance with respect to translation and rotation, uniqueness at every point on the MIZ, and nonheuristic handling of both convex and nonconvex regions (section 2). The second novel component is the development of the mathematics of an annulus as an analytically tractable idealized MIZ geometry, enabling us to quantitatively investigate the response of various spatial averaging formulas to changes in MIZ shape (section 3). The results in sections 2 and 3 support a recommendation to define MIZ width using streamlines through the solution to Laplace's equation within the MIZ and to average those results with respect to distance along the MIZ boundaries to yield the spatial average width. While the analyses in Strong (2012) and Strong and Rigor (2013) used these formulations, their mathematical justification was implicit and is here made rigorous. Finally, in section 4, we apply the streamline method to Arctic warm-season MIZ for 1979–2015 [a 3-yr extension of the results in Strong and Rigor (2013)], and we compare this extended time series to results from three alternative definitions that lack desirable mathematical properties or local width values but offer computational efficiency (one previously published, and two formulated for this study).

2. Definition of MIZ width

While the MIZ may be defined as the portion of the ice pack over which ocean waves significantly impact the dynamics of the sea ice cover (Wadhams 2000; Weeks 2010), several definitions of the MIZ based on sea ice concentrations have been used in recent studies founded on multidecade passive microwave satellite data (Strong 2012; Strong and Rigor 2013; Williams et al. 2014; Stroeve et al. 2016). Concentration-based definitions of the MIZ are also implemented operationally by the National Ice Center (NIC 2016). In most cases, concentration-based MIZ width is defined as the distance on the sphere between two concentration contours: typically 0.15, corresponding to the conventional ice edge (Comiso 2006); and 0.80, corresponding to what the World Meteorological Organization refers to as "close ice" (WMO 2009). We note that the methods for measuring width between the boundaries of the MIZ explored here do not require that the boundaries be defined by concentration thresholds, and they can applied in settings where the boundaries are defined by, for example, wave penetration or floe size (Williams et al. 2013).

TABLE 1. Entries indicate which mathematical properties (rows) are satisfied by four width definitions (columns), as detailed in section 2.

Property	Streamline	Meridian	Shortest path	Orthogonal geodesic
Invariance	Yes	No	Yes	Yes
Uniqueness	Yes	Yes	No	No
Generality	Yes	No	No	No

Once the MIZ boundaries have been identified, a rationale is needed for defining the path along which the MIZ width is to be measured. Strong (2012) and Strong and Rigor (2013), for example, measured width along streamlines through the solution to Laplace's equation within the MIZ, and we refer to this as the *streamline* definition. MIZ width has also been measured along meridians, and we refer to this as the *meridian* definition. Examples of the meridian definition in the literature often involve some form of time averaging prior to the width calculation. For example, Comiso and Zwally (1984) applied the meridian definition to MIZ boundaries identified in monthly mean concentrations, and Stroeve et al. (2016) averaged the latitude of the inner and outer edges of the MIZ at each meridian prior to calculating the distance between them. In medical imaging applications, Jones et al. (2000) note two other potential definitions: width defined as the shortest distance from a measurement point on one edge to the opposite edge, referred to here as the *shortest path* definition, and width defined as the distance along a straight line (geodesic on the sphere) that is orthogonal to the edge at the measurement point, referred to here as the *orthogonal geodesic* definition.

As a framework for considering the properties of these four definitions (streamline, meridian, shortest path, and orthogonal geodesic), we propose a set of three desirable mathematical properties for MIZ width:

- Invariance: the width at every point in the MIZ is invariant with respect to translation and rotation of the ice field.
- Uniqueness: the width at every point in the MIZ is uniquely defined.
- Generality: the width at every point in the MIZ generalizes to nonconvex shapes without requiring heuristic or arbitrary rules.

Table 1 indicates which of the abovementioned three properties are satisfied by the four width definitions,

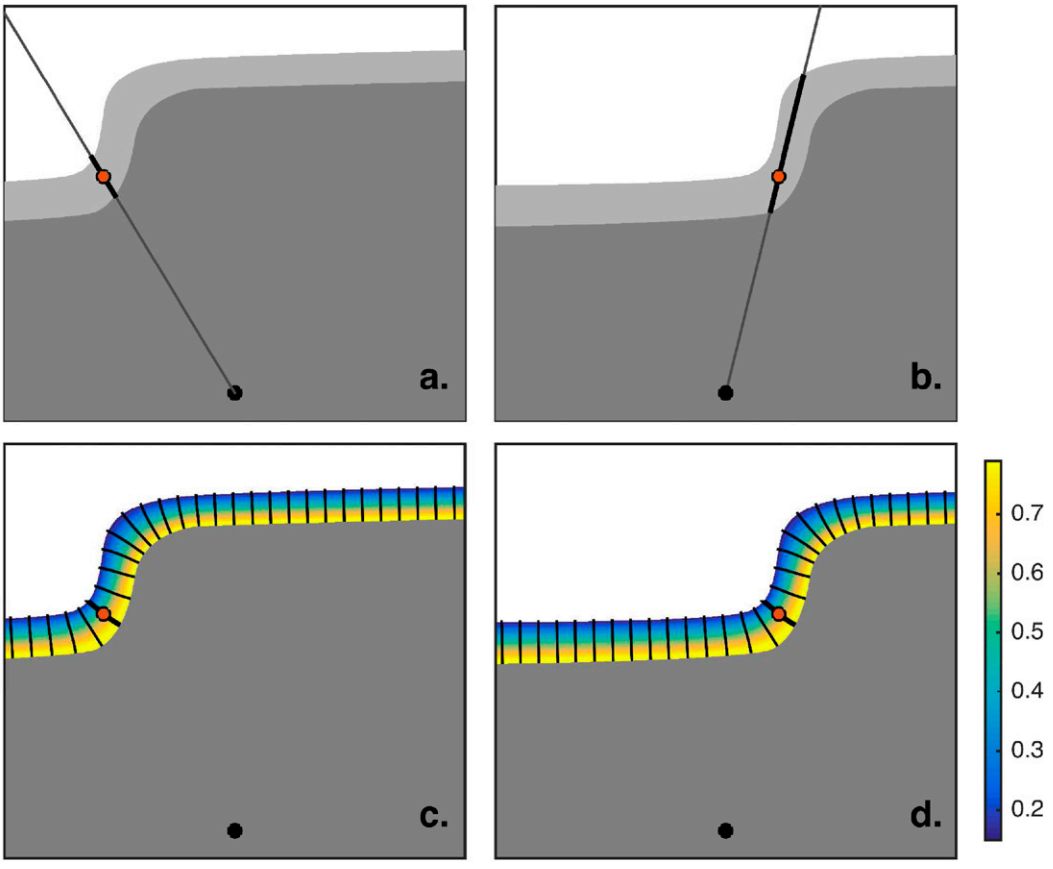

FIG. 2. (a) Dark gray shading represents a portion of an idealized inner pack ice region, and light gray shading represents a segment of an idealized MIZ. This panel is a polar stereographic projection with the pole indicated by the filled black circle near the lower edge of the panel, and the straight line indicates a meridian. The width of the MIZ through the red point as defined by the $\overline{\ell}_{\text{merid}}$ method is the length of the bold portion of the meridian. (b) As in (a), except the inner pack ice and MIZ have been translated to the right on the diagram with respect to the pole. (c) MIZ segment from (a) with the solution to Laplace's equation (shading) and a subset of the streamlines along which width is measured (black curves; streamline through the red point is bold). (d) As in (c), except the inner pack ice and MIZ have been translated to the right as in (b).

providing a summary of the remarks in sections 2a–c below.

a. Invariance

We view width as an intrinsic property that does not change if a shape is moved or rotated on the sphere. The streamline definition yields widths that are invariant with respect to translation and/or rotation because the solution to Laplace's equation provides width-defining streamlines that are determined by the shape of the MIZ and hence move with the MIZ, as illustrated by the idealized example in Figs. 2c,d. Results from the meridian method may change under translation and/or rotation as illustrated by the corresponding example in Figs. 2a,b (the shapes in Fig. 2 represent a single observation, but it could also represent MIZ boundaries diagnosed from time-averaged concentrations or boundaries constructed by time-averaging the latitude of the inner and outer MIZ edges). The shortest-path method and orthogonal-geodesic definitions are invariant with respect to translation and rotation because minimum-distance and orthogonality criteria are defined by the shape of, and hence move with, the MIZ.

b. Uniqueness

We view width at every point in the MIZ as an intrinsic property that does not change depending on whether width is measured *from* the point or *to* the point. Stated differently, every point on one boundary of the MIZ is mapped to one and only one point on the other boundary of the MIZ by a width measurement path. The uniqueness property assures an unambiguous width for every point in the MIZ and is provided by the streamline definition. As illustrated in Fig. 3b, for every

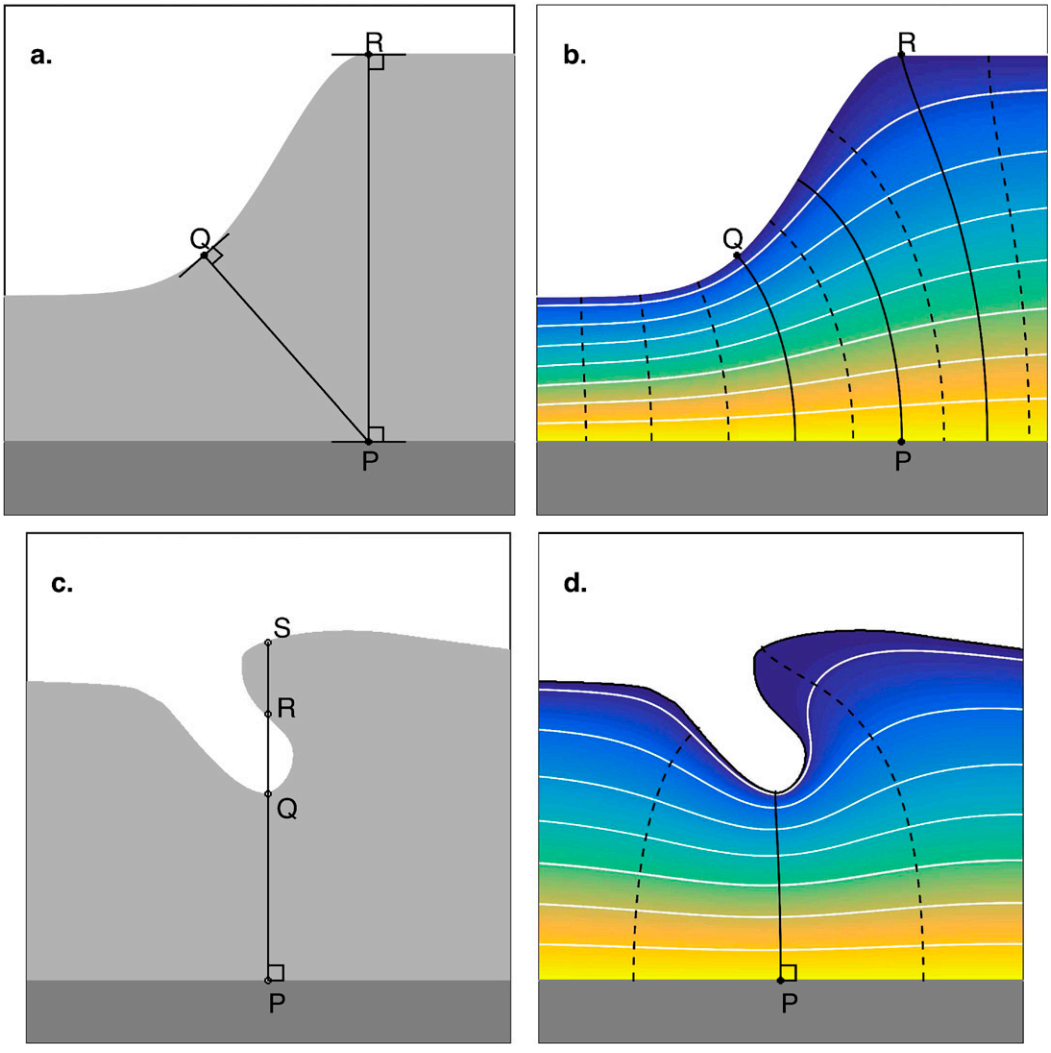

FIG. 3. (a) Dark gray shading represents a portion of an idealized inner pack ice region, and light gray shading represents a segment of an idealized MIZ in a stereographic projection with the origin at P so that geodesics intersecting P are projected as straight lines. (b) MIZ segment from (a) with the solution to Laplace's equation (shading) and a subset of the streamlines along which width is measured (black solid and dashed curves). (c) As in (a), but with a modified outer edge of the MIZ. (d) MIZ segment from (c) with the solution to Laplace's equation (shading) and a subset of the streamlines along which width is measured (black solid and dashed curves).

point in the MIZ (interior or boundary), the streamline definition provides exactly one width because every point is intersected by exactly one streamline. The width of the MIZ at point P in Fig. 3b, for example, is the arc length of the streamline intersecting P, and this value holds for all points along the streamline, including its point of intersection with the outer edge of the MIZ. The width at point P thus does not depend on whether the measurement is made from P or to P. The meridian definition also satisfies the uniqueness property because meridians do not intersect (except at the poles), and they uniquely map points between the two edges of the MIZ (unless curvature on an edge results in a meridian intersecting the same edge more than once; see discussion in section 2c).

As pointed out by Jones et al. (2000), seemingly natural or intuitive concepts such as the shortest distance and orthogonality to an edge work well in simple shapes, such as rectangles, but they can result in ambiguity and nonuniqueness when applied to regions with curved boundaries. To illustrate, consider the points $\{P, Q, R\}$ in Fig. 3a for the shortest-path definition. For point R, the shortest path across the MIZ is along the geodesic RP (geodesics intersecting P map to lines in this projection), but the shortest distance across the MIZ from P returns to Q (along the geodesic PQ) rather than to

R—an ambiguity Jones et al. (2000) refer to as *loss of reciprocity* or *loss of uniqueness* because there are at least two width measurement paths associated with point P. Similar ambiguities arise from the orthogonal-geodesic definition. For point Q in Fig. 3a, for example, the orthogonal geodesic across the MIZ is to point P, but the orthogonal geodesic from P returns to R rather than back to Q. These examples illustrate that the shortest-path and orthogonal-geodesic definitions do not satisfy the uniqueness property, meaning they yield results for a given point that may depend on the direction of measurement.

c. Generality

The actual MIZ features curvature and concavity, which may render it nonconvex, as seen in the example in Fig. 1b. Such nonconvexity may require arbitrary or heuristic decision-making for methods based on lines (or geodesics on the sphere) as illustrated by the idealized example in Fig. 3c. For point P, the path PS in Fig. 3c indicates the geodesic along which the shortest-path definition and the orthogonal–geodesic method would be applied, and it could additionally represent a segment of a meridian used for the meridian definition. This geodesic crosses the MIZ (segment PQ), leaves the MIZ (segment QR), and then reenters the MIZ (segment RS), rendering the width at point P ambiguous and not uniquely defined in the absence of an arbitrary rule. For the same MIZ configuration, the streamline definition has a unique width at P along the streamline (bold curve, Fig. 3d) that terminates at the outer edge of the MIZ, and additional streamlines objectively handle the surrounding nonconvexity by establishing nonoverlapping width measurement paths that do not leave the MIZ (e.g., dashed curves, Fig. 3d). Every point along the MIZ outer edge in Fig. 3d is mapped to a unique point on the inner edge by a streamline that connects the pair of points without leaving the MIZ, and the black solid and dashed curves in Fig. 3d are illustrative examples.

In summary, only the streamline definition provides the three mathematical properties of invariance, uniqueness, and generality (Table 1). Each of the other three definitions considered provide only one of the three properties. The remainder of the manuscript thus proceeds using the streamline definition, but in section 4 we consider some computationally efficient alternatives that can approximate results from the streamline method when calculated as a spatial average over the MIZ.

3. Definition of MIZ spatial average width

Now that we have width defined for every point on the MIZ interior and boundaries based on the streamline definition (denoted ℓ), we next consider how to formulate a summary statistic defining the MIZ spatial average width $\overline{\ell}$. The results in this section support a recommendation to use the MIZ spatial average width $\overline{\ell}_{\text{per}}$ as formulated by Strong (2012) and Strong and Rigor (2013), which is an average with respect to distance along the MIZ perimeter (meaning the inner and outer boundaries). Implicit in these two prior studies, the rationale for using $\overline{\ell}_{\text{per}}$ is that it is relatively insensitive to changes in MIZ shape that should intuitively leave the MIZ spatial average width unchanged. To illustrate, consider the MIZ shaded white in the eccentric annulus in Fig. 4a, which can be thought of as narrow on the right side and wide on the left side of the figure. If we envision moving the gray shaded inner pack ice region around within the circle, then an appropriately defined spatial average width should not respond markedly to these shifts because the areas of the inner pack ice and MIZ are not changing (i.e., some portions of the MIZ narrow while others comparably widen). Likewise, if we consider a circular MIZ and introduce sinusoidal modulations to the radius of one of its boundaries (here referred to as edge "waviness"; e.g., cf. Figs. 5a,d), an appropriately defined spatial average width should not respond markedly because some segments narrow while others comparably widen. Finally, if the inner radius is reduced (e.g., cf. Figs. 5b,c), then an appropriately defined spatial average width should respond approximately linearly.

To more rigorously investigate the properties of the spatial average width and support the recommendation to use $\overline{\ell}_{\text{per}}$, we now adopt an eccentric annulus as an idealized model of MIZ geometry and derive a formula for the arc length of the streamlines through the solution to Laplace's equation within the annulus. Associated notation and equations are established in section 3a, and we define $\overline{\ell}_{\text{per}}$ and five other candidate formulations for MIZ spatial average width in section 3b. Finally, we use the annulus to explore how results from the various width formulations respond to changes in eccentricity (section 3c), changes in the length of the inner and outer radii (section 3d), and changes in edge waviness (section 3e).

a. Annulus model and Laplace's equation

To illustrate how an annulus can provide a useful approximation to the MIZ, we show two actual MIZ configurations in Figs. 1a,b with corresponding annuli in Figs. 1d,e, respectively. In this approximation of the geometry, the MIZ is the annulus (white shading, Figs. 1d,e) defined by a unit radius outer circle at the MIZ–ocean interface and an inner circle at the inner pack ice–MIZ interface. The eccentric annulus enables us to use an analytical solution for Laplace's equation

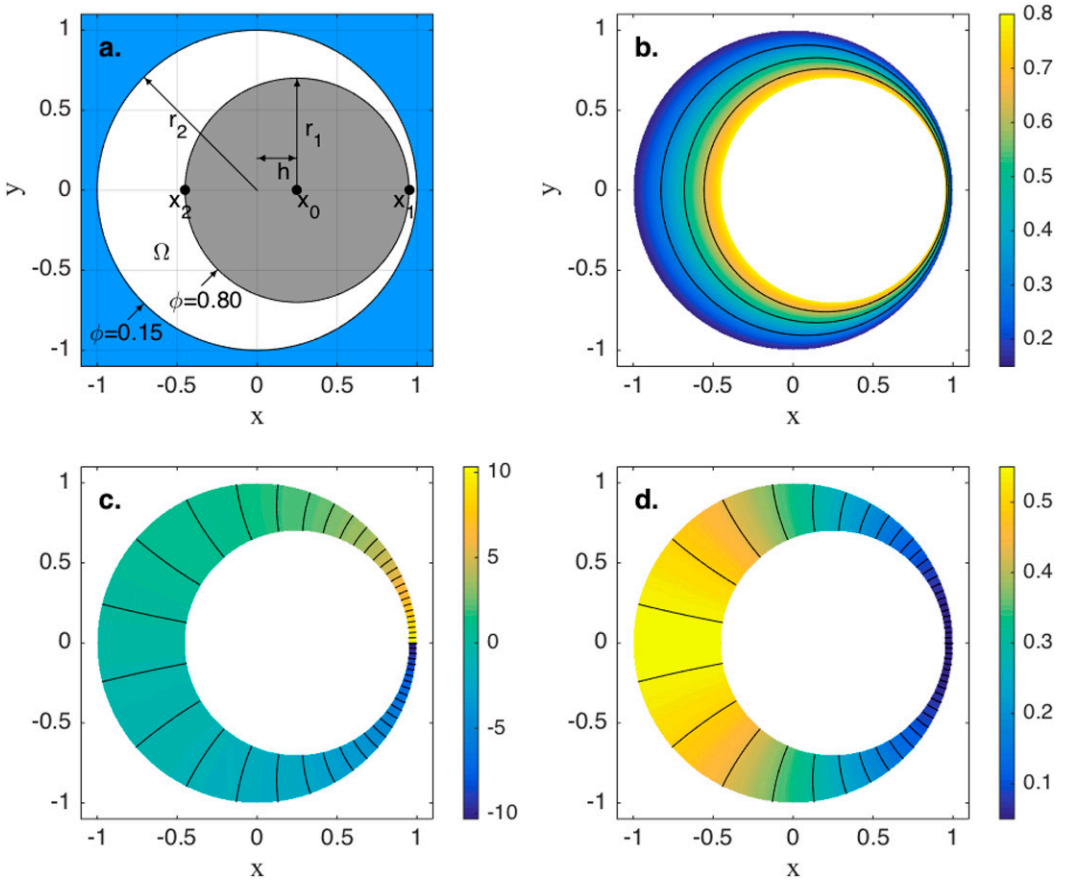

FIG. 4. (a) Schematic indicating notation for the eccentric annulus model: $r_1 = x_1 - x_0$ is the radius of inner circle, $r2 = 1$ is the radius of outer circle, the inner circle's center x_0 is offset from the origin by eccentricity h, and the annulus is denoted by Ω. (b) The real part of the solution to Laplace's equation within the annulus (ϕ), and (c) the imaginary part (ψ). (d) Shading indicates ℓ at a particular point defined by the arc length of the streamline (level set of ψ) through that point.

and to derive an explicit formula for the arc length of the associated streamlines (i.e., the MIZ width). Consider Laplace's equation $\nabla^2\phi = 0$ in the eccentric annulus model with the geometry shown in Fig. 4a. The function ϕ represents an idealized (smooth) sea ice concentration field within the MIZ modeled by the annulus with boundary conditions $\phi = 0.15$ on the outer edge (marginal ice/ocean interface) and $\phi = 0.80$ on the inner edge (marginal ice/inner pack ice interface). The outer edge of the marginal ice has radius $r_2 = 1$, the inner edge has radius r_1, and displacement of the inner pack ice center (x_0) from the origin defines the eccentricity h. Assume that the x–y plane in Fig. 4a represents a complex z plane with $z = x + iy$. Using a conformal mapping detailed in appendix A, Laplace's equation has a solution given by the complex potential

$$F(z) = \alpha \ln\left(\frac{z-a}{az-1}\right) + k, \tag{1}$$

where a is determined by the geometry of the annulus [x_1 and x_2, Fig. 4a; Eq. (A2)], and the constants $k = 0.15$ and $\alpha = (0.80 - 0.15)/\ln R_0$ are determined by the boundary conditions [R_0 is given by Eq. (A3)]. The real part of $F(z)$ is the potential (Fig. 4b) given by

$$\phi = \alpha \ln\left|\frac{z-a}{az-1}\right| + k, \tag{2}$$

and the imaginary part of $F(z)$ is the streamfunction (Fig. 4c) given by

$$\psi = \alpha \arg\left(\frac{z-a}{az-1}\right). \tag{3}$$

The solution ϕ represents an idealized sea ice concentration field for the MIZ that transitions smoothly between its boundary conditions (sea ice concentrations 0.80 on the pack ice edge and 0.15 on the ocean edge), as shown for an actual MIZ configuration in Fig. 1c.

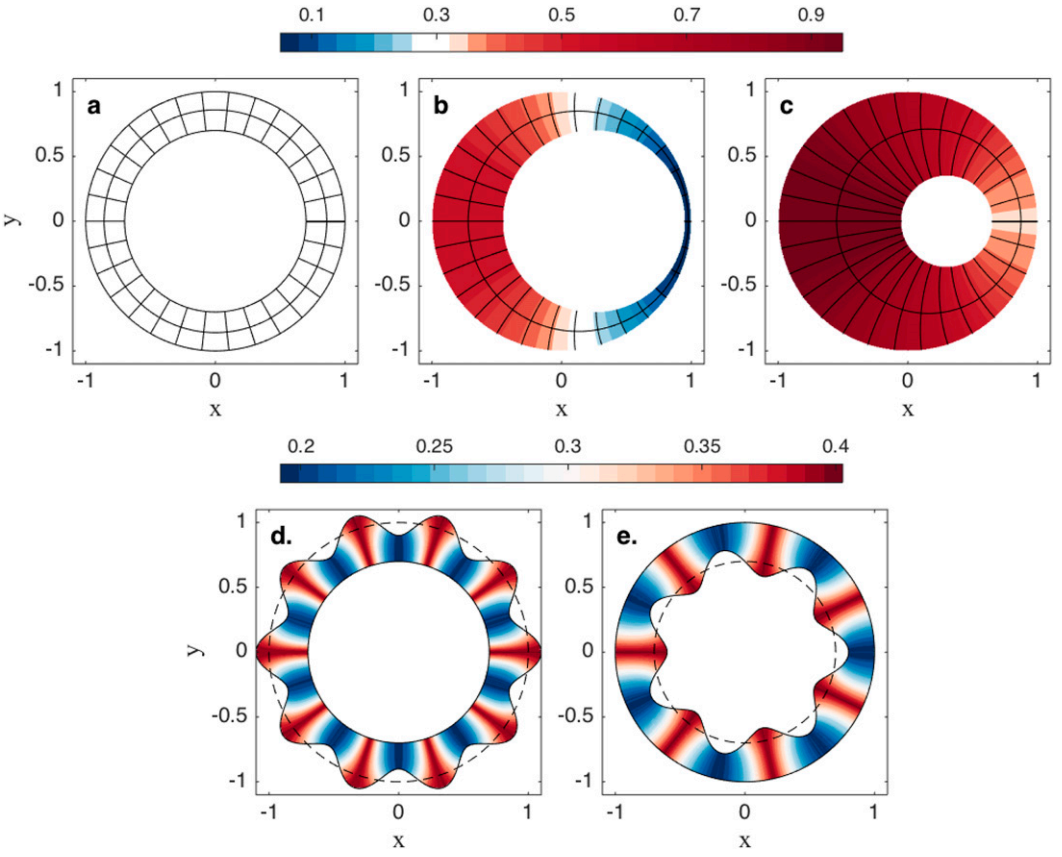

FIG. 5. Shading indicates ℓ at a particular point defined by the arc length of the streamline (level set of ψ) through that point. Each panel is an eccentric annulus example used to illustrate the effect of h and r_1: (a) $h = 0$, $r_1 = 0.7$. (b) $h = 0.25$, $r_1 = 0.7$, and (c) $h = 0.25$, $r_1 = 0.35$. Examples used to illustrate the effect of (d) waviness with $\{\delta = 0.1, f = 10, \overline{r_1} = 1, r_2 = 0.7, h = 0\}$ [see Eq. (14)], and (e) waviness on the inner edge with $\{\delta = 0.1, f = 7, r_1 = 1, \overline{r_2} = 0.7, h = 0\}$.

At a point in the annulus Ω, ℓ is defined as the arc length of the level set of ψ through that point (example streamline curves representing the level sets of ψ are shown by black contours in Figs. 1c,d, 4c). For the eccentric annulus model, we derived an explicit expression for ℓ as a function of ψ,

$$\ell(\psi_c/\alpha, a) = \begin{cases} \dfrac{a^2-1}{a\sin(\psi_c/\alpha)} \tan^{-1}\left[\dfrac{at - \cos(\psi_c/\alpha)}{\sin(\psi_c/\alpha)}\right]\Bigg|_{t=1}^{t=R_0}, & \text{if } \psi_c\alpha^{-1} \notin \{0, \pi\}, \\ 1 + x_2, & \text{if } \psi_c\alpha^{-1} = 0, \\ 1 - x_1, & \text{if } \psi_c\alpha^{-1} = \pi. \end{cases} \tag{4}$$

Shading in Fig. 4d shows width calculated at each point using Eq. (4).

b. *Candidate formulations for MIZ spatial average width*

The streamline definition provides a unique width at every point on the MIZ (interior and boundaries), so there is potential flexibility in how the MIZ spatial average width can be defined. For example, width could be averaged with respect to area over the MIZ, meaning averaged over the white shaded region for the example in Figs. 1a,b. Alternatively, width could be averaged with respect to distance along a curve, such as the outer boundary of the MIZ, meaning the boundary between blue and white shading for the examples in Figs. 1a,b. We define and investigate the properties of various candidate

TABLE 2. Average annulus width for six definitions of average width (definitions A–F). Columns indicate the associated formula, the equation number, and the average width for the examples in Figs. 5a–e.

Definition	Formula	Eq.	Fig. 5a	Fig. 5b	Fig. 5c	Fig. 5d	Fig. 5e
A: With respect to area	$\bar{\ell}_{\text{area}} = \frac{1}{A_\Omega}\int_\Omega \ell(x, y)\, dA$	(11)	0.300	0.405	0.702	0.298	0.293
With respect to distance							
B: Along outer perimeter	$\bar{\ell}_{\text{out}} = \frac{1}{L_{\text{out}}}\int_{\gamma_{\text{out}}} \ell(s)\, ds$	(6)	0.300	0.317	0.670	0.310	0.276
C: Along inner perimeter	$\bar{\ell}_{\text{in}} = \frac{1}{L_{\text{in}}}\int_{\gamma_{\text{in}}} \ell(s)\, ds$	(7)	0.300	0.280	0.623	0.272	0.303
D: Average of ℓ_{out} and ℓ_{in}	$\bar{\ell}_{\text{avg}} = \frac{1}{2}(\bar{\ell}_{\text{out}} + \bar{\ell}_{\text{in}})$	(8)	0.300	0.299	0.646	0.291	0.289
E: Weighted average of ℓ_{out} and ℓ_{in}	$\bar{\ell}_{\text{per}} = \frac{L_{\text{out}}\bar{\ell}_{\text{out}} + L_{\text{in}}\bar{\ell}_{\text{in}}}{L_{\text{out}} + L_{\text{in}}}$	(9)	0.300	0.302	0.657	0.300	0.300
F: Along level set of φ	$\bar{\ell}_{\phi^*} = \frac{1}{L_{\phi^*}}\int_{\gamma_{\phi^*}} \ell(s)\, ds$	(10)	0.300	0.300	0.650	N/A	N/A

formulations for MIZ spatial average width in this subsection, culminating in the recommendation to use width averaged with respect to distance along the perimeter $\bar{\ell}_{\text{per}}$ as in Strong (2012) and Strong and Rigor (2013). In Table 2 we consider five ways to average with respect to distance along a curve and one way to average with respect to area.

To establish notation, width averaged with respect to arc length s along the curve γ is

$$\bar{\ell}_\gamma = \frac{1}{L_\gamma}\int_\gamma \ell(s)\, ds, \tag{5}$$

where L_γ is the arc length of the curve γ. As a first specific case of Eq. (5), we consider width averaged with respect to arc length around the MIZ's outer boundary γ_{out},

$$\bar{\ell}_{\text{out}} = \frac{1}{L_{\text{out}}}\int_{\gamma_{\text{out}}} \ell(s)\, ds, \tag{6}$$

where L_{out} is the arc length of the outer boundary. When applied to the annulus, $L_{\text{out}} = 2\pi r_2$ for its circular outer perimeter (Fig. 4a). We can also consider width averaged with respect to arc length along the MIZ's inner boundary γ_{in},

$$\bar{\ell}_{\text{in}} = \frac{1}{L_{\text{in}}}\int_{\gamma_{\text{in}}} \ell(s)\, ds, \tag{7}$$

where L_{in} is the arc length of the inner boundary. When applied to the annulus, $L_{\text{in}} = 2\pi r_1$ for its circular inner boundary (Fig. 4a).

We might also consider the average of the outer and inner boundary results,

$$\bar{\ell}_{\text{avg}} = \frac{1}{2}(\bar{\ell}_{\text{out}} + \bar{\ell}_{\text{in}}). \tag{8}$$

The approach taken in Strong (2012) was to average with respect to arc length along the perimeter (meaning both the inner and outer MIZ boundaries), which is equivalently the weighted average of $\bar{\ell}_{\text{out}}$ and $\bar{\ell}_{\text{in}}$, where the weighting is the arc length of each boundary,

$$\bar{\ell}_{\text{per}} = \frac{L_{\text{out}}\bar{\ell}_{\text{out}} + L_{\text{in}}\bar{\ell}_{\text{in}}}{L_{\text{out}} + L_{\text{in}}}. \tag{9}$$

As a final example of averaging with respect to distance, we also consider an average with respect to arc length along a specific level set $\phi = \phi_*$ on the interior of the annulus (i.e., $0.15 < \phi_* < 0.80$),

$$\bar{\ell}_{\phi_*} = \frac{1}{L_{\phi_*}}\int_{\gamma_{\phi_*}} \ell(s)\, ds, \tag{10}$$

where L_{ϕ_*} is the arc length of the level set $\phi = \phi_*$. When applied to the annulus, L_{ϕ_*} is the circumference of a circle because the level sets of ϕ are circles (Fig. 4b).

For averages with respect to arc length along boundaries, we note that both the length $L_{\text{in(out)}}$ of the curve $\gamma_{\text{in(out)}}$ and the integral along this curve may grow without bound with increasing resolution. Here we assume that the resolution is limited, so the length of the curve $\gamma_{\text{in(out)}}$ is bounded.

Finally, because the streamline definition provides a width at every point on the MIZ (here Ω), we might also consider an average with respect to area,

$$\bar{\ell}_{\text{area}} = \frac{1}{A_\Omega}\int_\Omega \ell(x, y)\, dA, \tag{11}$$

where A_Ω is the total area of the annulus. This areal average is analogous to the average with respect to

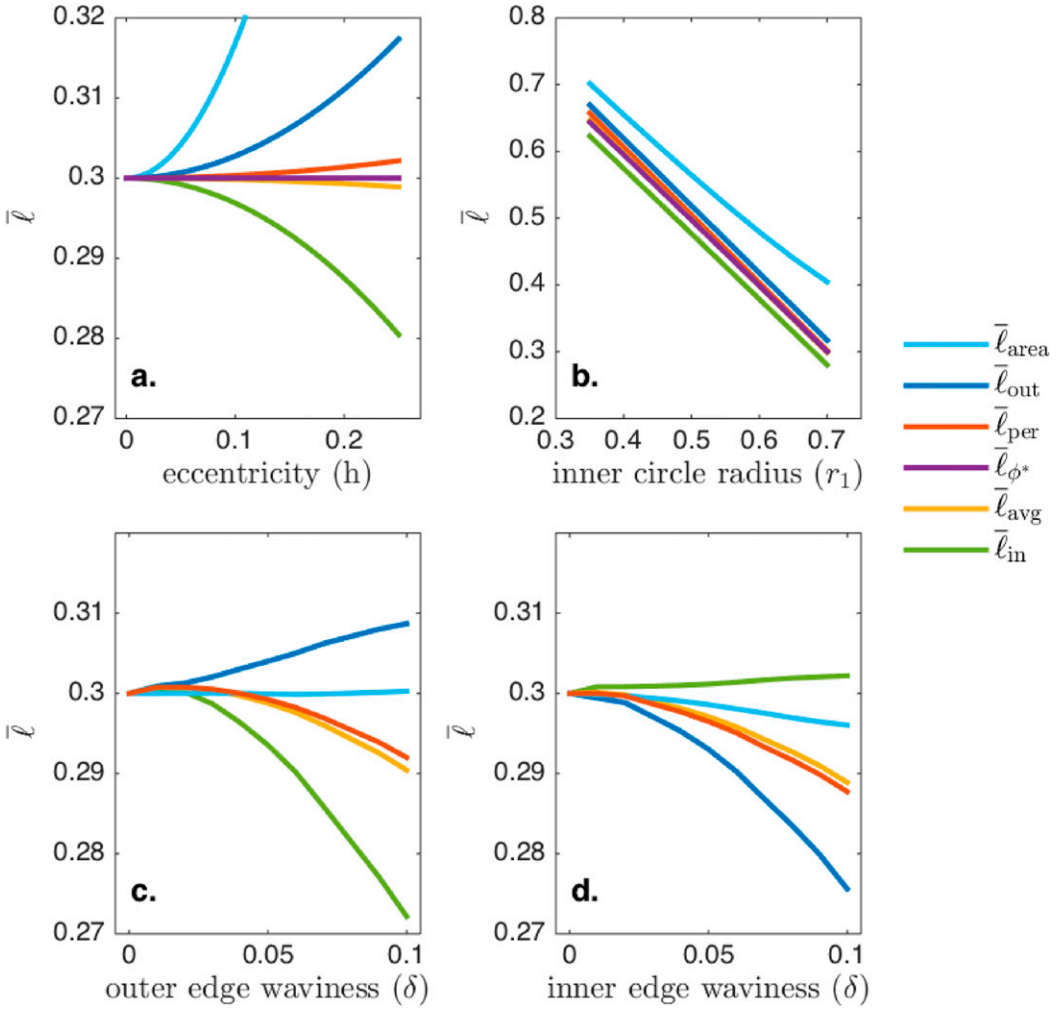

FIG. 6. For various definitions of MIZ spatial average width, dependence on (a) eccentricity, (b) inner circle radius, (c) waviness on the outer edge quantified by δ in Eq. (14), and (d) waviness on the inner edge quantified by δ in Eq. (14).

volume presented in application of the streamline definition in medical imaging (Jones et al. 2000).

c. *Response to eccentricity*

In this section, we examine how eccentricity affects results from the six candidate formulations for MIZ spatial average width. Our baseline case is the concentric annulus (Fig. 5a) whose average width ($\overline{\ell} = r_2 - r_1 = 0.3$) is consistent across all six candidate definitions (Table 2, column Fig. 5a).

Beginning with averages with respect to distance along the MIZ boundaries, we find that $\overline{\ell}_{\text{out}}$ and $\overline{\ell}_{\text{in}}$ respond oppositely to changes in eccentricity (Fig. 6a). For example, an eccentricity increase from $h = 0$ to $h = 0.25$ (see Figs. 5a,b) resulted in a 6% increase in $\overline{\ell}_{\text{out}}$ (from 0.300 to 0.317; Table 2, definition B) and a 7% decrease in $\overline{\ell}_{\text{in}}$ (from 0.300 to 0.280; Table 2, definition C). To illustrate why $\overline{\ell}_{\text{out}}$ and $\overline{\ell}_{\text{in}}$ respond oppositely to eccentricity, Fig. 7a shows ℓ as a function of angle $\beta \in [0, 2\pi)$ around the annulus's outer circle [denoted $\ell_{\text{out}}(\beta)$] and inner circle [denoted $\ell_{\text{in}}(\beta)$]. The functions $\ell_{\text{out}}(\beta)$ and $\ell_{\text{in}}(\beta)$ have the same range, intersecting at their maximum value $[\ell(\pi) = r_2 - r_1 + h]$ and minimum value $[\ell(0) = \ell(2\pi) = r_2 - r_1 - h]$, and we observe that $\ell_{\text{out}} \geq \ell_{\text{in}}$ for $\beta \in [0, 2\pi)$. The functions $\ell_{\text{out}}(\beta)$ and $\ell_{\text{in}}(\beta)$ resemble

$$\ell_{\cos}(\beta) = (r_2 - r_1) - h\cos(\beta), \tag{12}$$

which has average $r_2 - r_1$ (Fig. 7a). Figure 7b shows how ℓ_{out} and ℓ_{in} differ from $\ell_{\cos}$, illustrating that $\ell_{\text{out}} \geq \ell_{\cos}$ and $\ell_{\text{in}} \leq \ell_{\cos}$ for $\beta \in [0, 2\pi)$.

The average of the width results from the outer and inner perimeters $\overline{\ell}_{\text{avg}}$ is far less sensitive to eccentricity

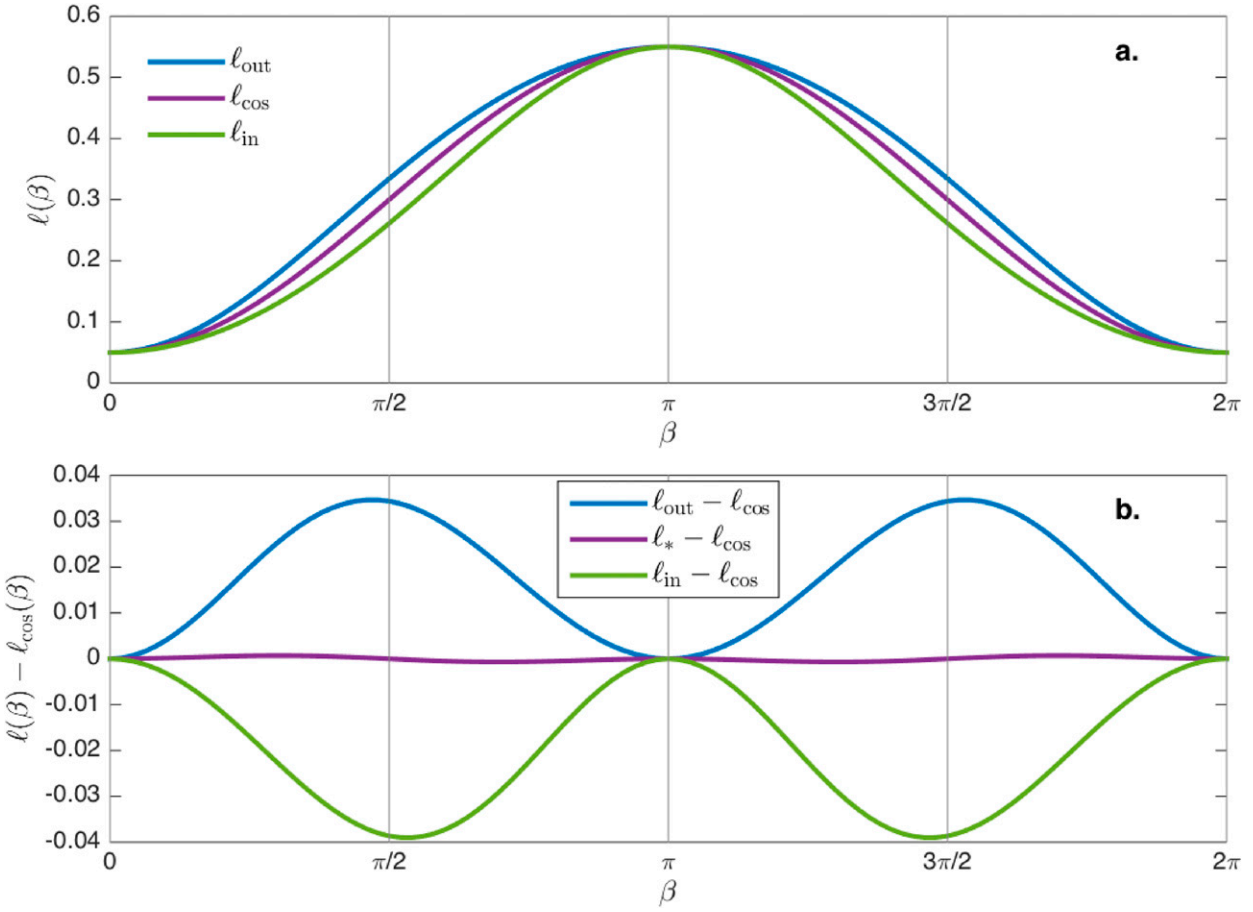

FIG. 7. (a) MIZ width as a function of ℓ_{out} and ℓ_{in}. Term ℓ_{cos} is Eq. (12) shown for reference. (b) Curves show how ℓ_{out}, ℓ_{in}, and ℓ_* differ from ℓ_{cos}.

(Fig. 6a), but it does decrease slightly with eccentricity because $\overline{\ell}_{in}$ decreases faster than $\overline{\ell}_{out}$ increases ($\overline{\ell}_{avg}$ is 0.300 and 0.299 for Figs. 5a,b, respectively; Table 2, D). This result encourages us to seek a width averaged with respect to arc length that is invariant with respect to eccentricity, meaning the average width takes the value $r_2 - r_1$ over the full range of h. The average with respect to distance along the inner and outer boundaries ($\overline{\ell}_{per}$) increases slightly with eccentricity (Fig. 6a). To understand this result, note that for the special case of the annulus, Eq. (9) becomes

$$\overline{\ell}_{per} = \frac{r_2\overline{\ell}_{out} + r_1\overline{\ell}_{in}}{r_2 + r_1} \tag{13}$$

because the perimeters are circles (Fig. 4a). The weight on $\overline{\ell}_{out}$ is larger than the weight on $\overline{\ell}_{in}$ by a factor of r_2/r_1, and $\overline{\ell}_{per}$ has values 0.300 and 0.302 for Figs. 5a,b, respectively (Table 2, definition E).

Probing further for a definition of average width that is invariant with respect to eccentricity, we consider averages with respect to distance along level sets of ϕ on the interior of the annulus [Eq. (10)]. The width averaged with respect to distance along circular level sets of ϕ is continuous and monotonic over the range $0.15 \le \phi \le 0.80$ (appendix B). Hence, there exists a unique level set of ϕ (denoted ϕ_*) along which we can average $\ell(\beta)$ to yield the width $r_2 - r_1$ for the given radii and eccentricity $\{r_1, r_2, h\}$. To find ϕ_*, we use a simplex search method (Lagarias et al. 1998) to minimize $|\overline{\ell} - (r_2 - r_1)|$, and we use $\overline{\ell}_{\phi_*}$ to denote the average width along the level set $\phi = \phi_*$. For the example in Fig. 5b we have $\{r_1 = 1, r_2 = 0.7, h = 0.25, \phi_* = 0.43\}$ and $\overline{\ell}_{\phi_*} = 0.300$ at $h \in \{0, 0.25\}$ (Table 2, definition F). From visual inspection of the resultant graph in Fig. 6a, $\overline{\ell}_{\phi_*}$ appears invariant with respect to h, yet it has order 10^{-6} departures from $r_2 - r_1$ over the range $0 < h < 0.25$ (Fig. B1)—a discrepancy too large to attribute to numerical error. More importantly, ϕ_* depends strongly on the radii themselves. For example, Fig. 5c differs from Fig. 5b by a halving of r_1, resulting in a reduction of ϕ_* from 0.43 to 0.30. There is thus not a single ϕ_* that is

applicable to all ice configurations, even in the eccentric annulus case, so it is unclear how the ϕ_* concept could be applied to satellite data without arbitrariness.

Finally, we consider the average with respect to area $\overline{\ell}_{\text{area}}$ [Eq. (11)], finding it to be strikingly sensitive to eccentricity. To illustrate, increasing the eccentricity from $h = 0$ to $h = 0.25$ (Fig. 5b), we see that $\overline{\ell}_{\text{area}}$ responds strongly because, as the inner circle shifts off center, the portions of the annulus that are becoming wider are also occupying a larger area (cf. Figs. 5a,b, where $\overline{\ell}_{\text{area}} = 0.300$ for Fig. 5a, while $\overline{\ell}_{\text{area}} = 0.405$ for Fig. 5b). Numerical results for a particular choice of parameters of the annulus, demonstrating the dependence of $\overline{\ell}_{\text{area}}$ on eccentricity, are shown in Table 2A. This rapid increase of $\overline{\ell}_{\text{area}}$ with eccentricity is shown in Fig. 6a, where the endpoints of the $\overline{\ell}_{\text{area}}$ curve correspond to the change from Fig. 5a (eccentricity $h = 0$) to Fig. 5b (eccentricity $h = 0.25$).

d. Response to size of inner pack ice and total ice

Here we examine for zero and nonzero eccentricity how results from the candidate formulations for MIZ spatial average width respond to changes to the inner radius length relative to the outer radius length. A smaller inner radius will result in a larger average width for any reasonable definition. With zero eccentricity, all definitions yield $\overline{\ell} = r_2 - r_1$ (Table 2, definitions A–F, column Fig. 5a), indicating a linear and consistent response to changes in r_1. Eccentricity $h > 0$ alters this consistent result across the six definitions. To illustrate, the annuli in Figs. 5b,c have the same nonzero eccentricity ($h = 0.25$) and the inner radius in Fig. 5c has been halved to $r_1 = 0.35$. All six definitions explored here yield a larger average width for Fig. 5c than for Fig. 5b (Table 2, definitions A–F), but the values in column Fig. 5c vary among the formulations. The dependence of MIZ spatial average width on the inner radius is approximately linear except for $\overline{\ell}_{\text{area}}$ (Fig. 6b).

e. Response to sinusoidal modulation of the boundaries

The inner and outer boundaries of the observed MIZ depart significantly from circularity (e.g., Figs. 1a,b). Here we examine how results from the six MIZ spatial average width definitions respond to this kind of enhanced edge curvature, here referred to as waviness. To begin, we perturb the outer boundary in Fig. 5a with a sinusoidal fluctuation written in polar coordinates as

$$r_2 = 1 + \delta \cos(f\beta), \tag{14}$$

where $0 \le \beta < 2\pi$ is the angular coordinate, $\delta = 0.1$ is the amplitude of the perturbation, and $f = 10$ is the frequency of the perturbation (Fig. 5d). These values for δ and f are chosen to capture scales of variation salient in the observed examples (cf. Figs. 1a,b, 5d,e). The introduction of this waviness caused the area to increase by $\pi\delta^2/2$, which is approximately 1%. Waviness resulted in width decreases along the majority of the inner boundary (blue shading, Fig. 5d) and a 9% decrease in $\overline{\ell}_{\text{in}}$ to 0.272 (Table 2, definition C; cf. columns Figs. 5a,d). Absolute changes in $\overline{\ell}_{\text{area}}$, $\overline{\ell}_{\text{out}}$, $\overline{\ell}_{\text{avg}}$, and $\overline{\ell}_{\text{per}}$ were no larger than 3% (Table 2, definitions A, B, D, E; cf. columns Figs. 5a,d). The very small change in $\overline{\ell}_{\text{area}}$ in response to boundary waviness is especially notable in contrast to this formulation's sensitivity to eccentricity highlighted in section 2c.

Next we construct Fig. 5e by perturbing the radius of the inner circle as in Eq. (14) but with $f = 7$, chosen so that the wavelength of the perturbation is the same in Figs. 5d,e (i.e., $2\pi/10 = 2\pi 0.7/7$). This waviness caused the area to decrease by $\pi\delta^2/2$, which is approximately 1%, and it produced average width results essentially opposite to results associated with waviness on the outer circle. Specifically, widths decreased along the majority of the outer boundary (blue shading, Fig. 5e) and $\overline{\ell}_{\text{out}}$ decreased by 8% to 0.276 (Table 2, definition C; cf. columns Figs. 5a,e). Absolute changes in $\overline{\ell}_{\text{area}}$, $\overline{\ell}_{\text{out}}$, $\overline{\ell}_{\text{avg}}$, and $\overline{\ell}_{\text{per}}$ were no larger than 4% (Table 2, definitions A, C, D, E; cf. columns Figs. 5a,e).

The abovementioned analysis indicates that lengthening of one edge by waviness tends to modestly increase the average width measured along the wavy edge and more substantially decrease the average width measured along the nonwavy edge for all formulations. This effect is reduced by averaging the inner and outer boundary results (i.e., using $\overline{\ell}_{\text{per}}$ or $\overline{\ell}_{\text{avg}}$) as further illustrated in Figs. 6c,d, respectively, where waviness is progressively increased in amplitude. As noted above, we chose the wavelengths for the examples in Figs. 5d,e to represent variations salient in observations. Exploring the effects over the ranges $0 \le \delta \le 0.2$ and $2 \le f \le 12$, the decrease in width on the nonwavy edge appears robust, but the width measured from the wavy edge can decrease monotonically for more extreme values of f (not shown).

f. Summary of sensitivity to MIZ shape

This subsection is a summary of findings in the preceding three subsections. As eccentricity increases, width averaged with respect to distance increases for the outer boundary and decreases for the inner boundary (section 3c). This sensitivity is considered undesirable and is largely eliminated by combining the inner and outer boundary results either as an arithmetic mean ($\overline{\ell}_{\text{avg}}$) or weighted average ($\overline{\ell}_{\text{per}}$) as in Strong (2012) and Strong and Rigor (2013). For changes in the inner radius,

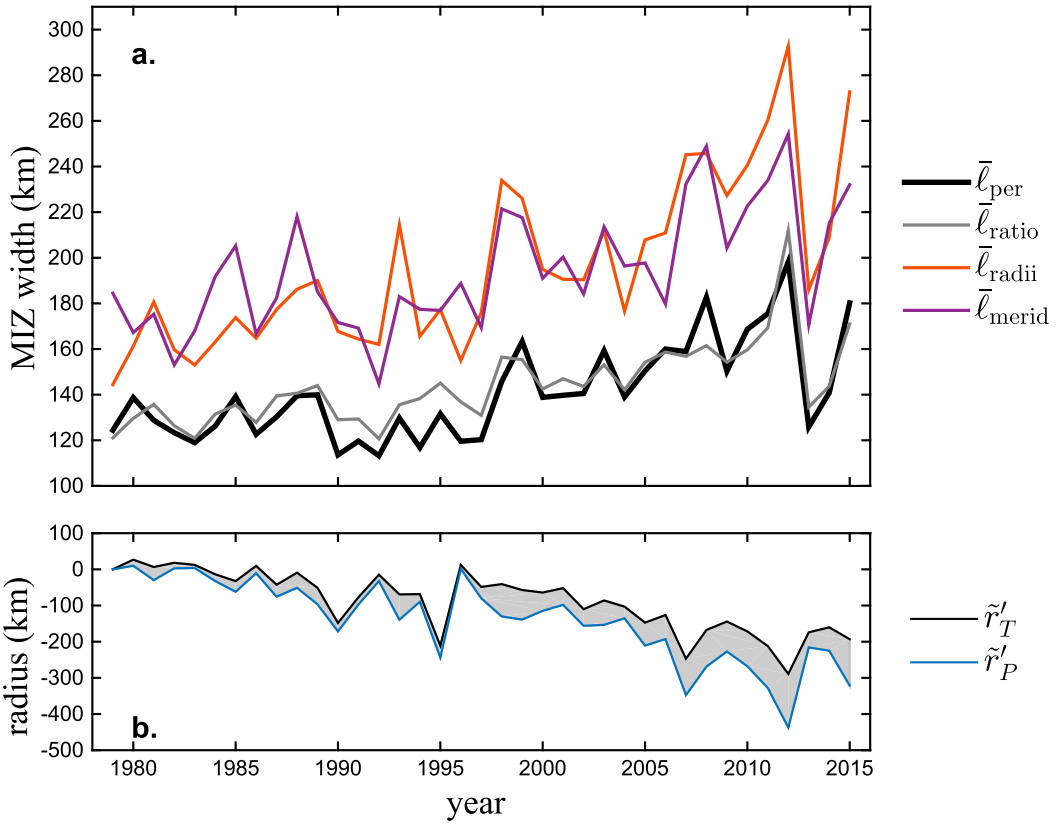

FIG. 8. (a) MIZ average width for July–September based on analysis of satellite data. For the streamline definition, $\overline{\ell}_{\rm per}$ is the average with respect to distance along the inner and outer boundaries of the MIZ. Other curves are methods that yield mean widths with less computational expense than the streamline method. (b) Terms $\tilde{r}_T$ and $\tilde{r}_P$, shown as anomalies relative to their values in 1979.

all formulations had an approximately linear response as we would desire, with $\overline{\ell}_{\rm area}$ having the largest departure from linearity (section 3d). Introducing waviness on one boundary, width averaged with respect to distance along the wavy boundary increased whereas width averaged with respect to distance along the smooth boundary decreased (section 3e). This sensitivity is considered undesirable and is substantially lessened by combining the inner and outer boundary results either as $\overline{\ell}_{\rm avg}$ or $\overline{\ell}_{\rm per}$. Considering the findings summarized here collectively, we recommend the weighted average $\overline{\ell}_{\rm per}$ as used in Strong (2012) and Strong and Rigor (2013).

4. Application to satellite data

The preceding sections 2 and 3 motivate use of the streamline definition of MIZ width, with a spatial average width defined by averaging with respect to distance along both MIZ boundaries ($\overline{\ell}_{\rm per}$). In section 4a below, we apply the $\overline{\ell}_{\rm per}$ formulation to daily warm-season (July–September) sea ice concentrations from the Climate Data Record (CDR) of Passive Microwave Sea Ice Concentration, which is a blending of different algorithms intended to produce a consistent record over time (Meier et al. 2012). This CDR analysis, presented in section 4a, replicates and extends a subset of the results from Strong and Rigor (2013), who used the CDR covering 1988–2012 and bootstrap algorithm concentrations covering 1979–2012. We focus on the Arctic warm season because it features a large range of widths and a widening trend that illustrate the extent to which $\overline{\ell}_{\rm per}$ can be approximated by computationally efficient alternatives (section 4b) that either lack desirable mathematical properties or do not provide local width information.

a. MIZ spatial average width from streamline definition

The bold curve in Fig. 8a is the recommended $\overline{\ell}_{\rm per}$ formulation and is an extension of the results presented in Strong and Rigor (2013). A widening trend amounting to approximately 40% is seen for 1979–2015, slightly larger than the 37% widening trend previously found applying the same method to the shorter period 1979–2012 (Strong and Rigor 2013). The extension of the

analysis here reveals a return to widths representative of the 1980s during the 2-yr period 2013–14, with wider widths once again during the final year of the record. The two sequential years of narrower MIZ (2013 and 2014) are consistent with observed 25%–33% increases in sea ice volume in autumn 2013 and 2014 relative to 2010–12 (Tilling et al. 2015).

The widening trend is consistent with the decline in the inner pack ice area outpacing the decline in total ice area. To visualize this, we plot the effective radius of the total ice area ($\tilde{r}_T$) and the effective radius of the inner pack ice area ($\tilde{r}_P$) together in Fig. 8b (the effective radius is the radius of a circle with the same area as the ice). The $\tilde{r}_P$ decline outpaced the $\tilde{r}_T$ decline with both trending downward ($-89\,\mathrm{km\,decade^{-1}}$ for $\tilde{r}_P$ vs $-63\,\mathrm{km\,decade^{-1}}$ for $\tilde{r}_T$).

b. *MIZ spatial average width from alternative definitions*

We now consider three alternative definitions of MIZ spatial average width that are less computationally expensive than $\overline{\ell}_{\mathrm{per}}$ while still emphasizing that $\overline{\ell}_{\mathrm{per}}$ remains our recommended definition and formulation because these alternatives either lack desirable mathematical properties or do not provide local width values.

For a rectangle, width is area divided by length. Extending that concept to the present context, the average width of the MIZ could be defined using a ratio of area to boundary length,

$$\overline{\ell}_{\mathrm{ratio}} = \frac{A_\Omega}{\overline{L}}, \tag{15}$$

where $\overline{L}$ is the average of the MIZ outer boundary and inner boundary lengths, and A_Ω is the area of the MIZ. While $\overline{\ell}_{\mathrm{ratio}}$ does not provide local values for MIZ width, it yields results very similar to $\overline{\ell}_{\mathrm{per}}$ as seen in Fig. 8a ($r^2 = 0.92$; bias 3.2 km), and it can be used as a computationally efficient alternative to the streamline method for 25-km-resolution satellite data if only the spatial average is needed. If substantially finer-resolution satellite data are used for $\overline{\ell}_{\mathrm{ratio}}$, then the boundary may need to be coarsened to a resolution close to 25 km if its length increases substantially when resolved at finer resolutions (note that boundary arc length appears in the denominator of $\overline{\ell}_{\mathrm{ratio}}$). In addition to being computationally efficient and conceptually simple, $\overline{\ell}_{\mathrm{ratio}}$ features invariance with respect to translation and rotation, and is applicable to convex and nonconvex MIZ shapes.

We can also consider a definition of MIZ spatial average width using the effective radii defined at the end of section 4a, written as

$$\overline{\ell}_{\mathrm{radii}} = \tilde{r}_T - \tilde{r}_P. \tag{16}$$

This formulation, based on the difference in effective radii, produced widths approximately 39% larger than $\overline{\ell}_{\mathrm{per}}$ (Fig. 8a). To understand this result, we use the close agreement of $\overline{\ell}_{\mathrm{per}}$ and $\overline{\ell}_{\mathrm{ratio}}$ noted above to write

$$\frac{\overline{\ell}_{\mathrm{radii}}}{\overline{\ell}_{\mathrm{per}}} \approx \frac{\overline{\ell}_{\mathrm{radii}}}{\overline{\ell}_{\mathrm{ratio}}} = \frac{\tilde{r}_T - \tilde{r}_P}{\left(\dfrac{A_T - A_P}{\overline{L}}\right)} = \frac{\overline{L}}{\pi(\tilde{r}_T + \tilde{r}_P)}, \tag{17}$$

where A_T is the total ice area and A_P is the inner pack ice area. The right side of Eq. (17) is unity when the average of the inner and outer MIZ boundary lengths ($\overline{L}$) is equal to the effective circumference $\pi(\tilde{r}_\mathrm{T} + \tilde{r}_\mathrm{P})$, which is the average of the circumferences associated with the effective radii $\tilde{r}_\mathrm{T}$ and $\tilde{r}_\mathrm{P}$. Casting the ice areas as equivalent-area circles in the $\overline{\ell}_{\mathrm{radii}}$ formulation minimizes their perimeters per the isoperimetric inequality, so $\pi(\tilde{r}_T + \tilde{r}_P)$ is a lower bound for $\overline{L}$. We find in satellite data that the observed $\overline{L}$ is approximately 1.3 times larger than $\pi(\tilde{r}_T + \tilde{r}_P)$, explaining the finding $\overline{\ell}_{\mathrm{radii}}/\overline{\ell}_{\mathrm{ratio}} \approx \overline{\ell}_{\mathrm{radii}}/\overline{\ell}_{\mathrm{per}} \approx 1.3$. Thus, while the quantity $\overline{\ell}_{\mathrm{radii}}$ is computationally efficient, invariant with respect to translation and rotation, and applicable to convex and nonconvex shapes, casting the ice areas as equivalent circles tends to inflate $\overline{\ell}_{\mathrm{radii}}$ relative to $\overline{\ell}_{\mathrm{per}}$ (in this case by 39%).

For the third and final computationally efficient alternative, we consider here the MIZ spatial average width calculation that was applied to the Antarctic satellite record in Stroeve et al. (2016). This is the meridian definition discussed in section 2 implemented with a time-averaging operation. For this definition of the MIZ average width ($\overline{\ell}_{\mathrm{merid}}$), the latitudes of the inner and outer MIZ edges were recorded on each meridian and then averaged over a month, the distance between the monthly average latitudes was calculated for each meridian, and then those results were averaged across all meridians (note that the distance between the average latitudes of the boundaries on a meridian is equivalent to the average distance between the boundaries on that meridian because differencing is linear). This definition is computationally efficient to implement and makes sense given the tendency for sea ice to expand out away from the poles, especially in the Antarctic, where the ice field is more radially symmetric than the Arctic. Our Arctic $\overline{\ell}_{\mathrm{lati}}$ analysis yielded results similar to $\overline{\ell}_{\mathrm{radii}}$ (Fig. 8a), which is consistent with the conceptual similarity of the definitions (i.e., we might expect the effective radius to be similar to the distance from the pole to the average MIZ edge). Also, the effect illustrated by the idealized example in Fig. 2 tends to increase $\overline{\ell}_{\mathrm{merid}}$

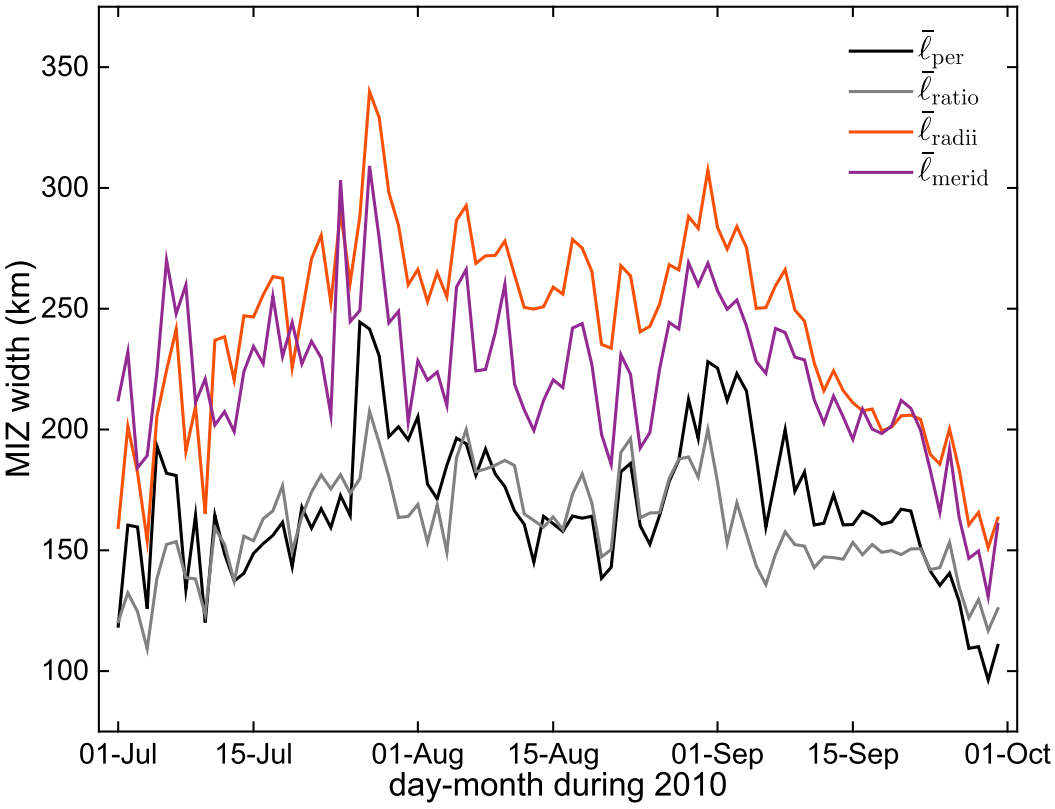

FIG. 9. As in Fig. 8a, but shown daily for July–September 2010.

relative to $\overline{\ell}_{\mathrm{per}}$. Thus, $\overline{\ell}_{\mathrm{merid}}$ is computationally efficient and yields results similar to $\overline{\ell}_{\mathrm{radii}}$ ($r = 0.85$; mean absolute difference of 20 km), but the use of meridians means that $\overline{\ell}_{\mathrm{merid}}$ can be altered by translation or rotation as noted in section 2, and $\overline{\ell}_{\mathrm{merid}}$ tends to be larger than $\overline{\ell}_{\mathrm{per}}$.

To complement the seasonal mean results presented above, we present a daily comparison of $\overline{\ell}_{\mathrm{per}}$ to the three alternative definitions ($\overline{\ell}_{\mathrm{radii}}$, $\overline{\ell}_{\mathrm{ratio}}$, and $\overline{\ell}_{\mathrm{merid}}$). We chose 2010 as an example to correspond to the season in which Fig. 1b occurred. On a daily basis, the relationships between the results of the different definitions (Fig. 9) are similar to the seasonal mean relationships (Fig. 8a) in terms of the relative size of the MIZ width (i.e., $\overline{\ell}_{\mathrm{radii}} \approx \overline{\ell}_{\mathrm{merid}} > \overline{\ell}_{\mathrm{per}} \approx \overline{\ell}_{\mathrm{ratio}}$).

5. Summary and discussion

The width of the MIZ is a fundamental length scale for polar physical and biological dynamics, and a variety of width definitions have emerged in the literature over the past three decades. The streamline definition recommended here defines width as the arc length of streamlines through the solution of Laplace's equation within the MIZ, and it features invariance with respect to translation and rotation, uniqueness at every point on the MIZ, and generality to nonconvex shapes. Our recommended definition for MIZ spatial average width, tested by sensitivity analyses using an annulus as an analytically tractable idealized MIZ geometry, is the average taken with respect to distance along the MIZ boundaries. We applied the recommended definitions to the warm-season (July–September) Arctic satellite record (1979–2015), extending the previously reported widening trend analysis by 3 yr and updating the total widening to 40%. The three most recent years in the record featured notable MIZ narrowing during two sequential years (2013–14), consistent with observed 25%–33% increases in sea ice volume in autumn 2013 and 2014 relative to the 2010–12 mean (Tilling et al. 2015).

Three computationally efficient alternatives to the streamline-based MIZ spatial average width were presented for comparison over the satellite record. While some approximations such as the difference in effective radii ($\overline{\ell}_{\mathrm{radii}}$) exceeded the streamline-based results by up to 39%, MIZ area divided by the average of the inner and outer boundary lengths ($\overline{\ell}_{\mathrm{ratio}}$) yielded results that were very similar to the streamline method ($r = 0.92$; bias 3 km) and might thus provide a computationally efficient alternative to the streamline method if only the

spatial average statistic is needed. In addition to being computationally efficient and conceptually simple, $\overline{\ell}_{\text{ratio}}$ features invariance with respect to translation and rotation, and is applicable to convex and nonconvex MIZ shapes. However, if substantially finer-resolution satellite data are used for $\overline{\ell}_{\text{ratio}}$, then the boundary may need to be coarsened to a resolution close to the nominally 25-km resolution used here in order to achieve results comparable to the streamline method. We speculate that $\overline{\ell}_{\text{ratio}} \approx \overline{\ell}_{\text{per}}$ would hold if applied to the Antarctic satellite record as well, but the agreement $\overline{\ell}_{\text{ratio}} \approx \overline{\ell}_{\text{per}}$ could weaken as the MIZ evolves during future decades.

All three computationally efficient alternatives indicated statistically significant widening trends, suggesting that a broad range of reasonable definitions will agree on the presence or absence of trends, and in some cases the associated percent change (widening amounted to 33% for $\overline{\ell}_{\text{merid}}$ and 34% for $\overline{\ell}_{\text{ratio}}$). The analysis here suggests that results from the streamline method would agree with the $\overline{\ell}_{\text{merid}}$ results in Stroeve et al. (2016) with regard to dataset-dependent presence or absence of trends in Antarctic MIZ width. The $\overline{\ell}_{\text{radii}}$ time series, in contrast, indicated a substantially larger—60%—widening trend in part because the $\overline{\ell}_{\text{radii}}$ formulation minimizes the perimeters of the ice areas per the isoperimetric inequality as discussed in section 4b. The variance of $\overline{\ell}_{\text{radii}}$ is also larger than the variance of $\overline{\ell}_{\text{per}}$ by a factor of 2.2.

In summary, we recommend using the streamline definition of MIZ width because of its mathematical properties (invariance, uniqueness, and generality), and we recommend defining MIZ spatial average as an average with respect to distance along the MIZ boundaries based on results of our sensitivity analyses. The basis for these recommendations is objective and mathematical. The context for these recommendations spans both MIZ physical dynamics and climate science research. When multidecadal time series are constructed, the focus is on spatiotemporal changes, including trends indicating the response of the ice field to natural variability and anthropogenic forcing. At the smaller spatial and temporal scales of MIZ physical dynamics, Laplace's equation can be thought of as a steady-state heat equation, in which case its solution would define a smooth and monotonic decrease in temperature from the outer to inner edge of the MIZ that could in principle thermodynamically force a concentration increase in the same direction. Laplace's equation is also the steady-state solution to Fick's second law and thus defines a concentration field that would arise from a constant source (constant concentration) diffusing inward from the MIZ inner edge with a constant melting rate at the MIZ outer edge. In this way, while sea ice concentration does not formally obey it, Laplace's equation is linked to potentially relevant thermodynamic and dynamic processes as a steady-state solution in the context of heat and diffusion. Advection is important in the actual MIZ, and this is not explicitly considered in Laplace's equation. Ultimately, the goal of using Laplace's equation is not to represent the sea ice physics, but to provide an idealized sea ice concentration field whose streamlines provide an objective definition of width satisfying invariance, uniqueness, and generality.

We now offer some remarks on the fact that the streamline definition uses the arc length of streamlines to define MIZ width as opposed to, say, great circles or straight lines on a stereographic projection. It is the use of streamlines that enables the streamline definition to simultaneously satisfy the properties of invariance, uniqueness, and generality. For simple planar shapes like rectangles, the width measurement path is a straight-line orthogonal to the opposing edges, yet the curvilinear streamline and planar straight-line definitions of width are not entirely unrelated. First, observe that the planar straight-line width for a rectangle is the shortest distance side to side across the shape, meaning a line orthogonal to two opposing edges. The streamlines through the solution to Laplace's equation are also (by definition) orthogonal to the boundaries, and they thus take on curvature where the MIZ departs from simple rectangular (or spherical quadrangle) geometry (e.g., consider Fig. 3b). Second, we found that $\overline{\ell}_{\text{per}}$ yielded a value very close $\overline{\ell}_{\text{ratio}}$, where the latter yields the width of a rectangle by the definition of a rectangle's area. There is one additional, more subtle connection between the rectangular and curvilinear definitions, and it relates to the concept of width as a shortest distance. The streamlines also represent a form of the shortest distance between the edges of the MIZ, not on the physical surface of the spherical earth where kilometers of arc length are measured during application of the definition, but on the three-dimensional mathematical surface defined by the concentration field that solves Laplace's equation (i.e., in a three-dimensional space where concentration is the third spatial dimension orthogonal to the plane of the stereographic projection). Because a streamline everywhere follows the gradient of the concentration (i.e., is everywhere orthogonal to the level sets of concentration), each streamline is a so-called *minimal geodesic* defining the shortest path between the MIZ edges if distance were to be measured along the three-dimensional concentration surface. This three-dimensional mathematical concentration surface does not exist in physical space, and we emphasize that MIZ width is the arc length of the streamline along the surface of the earth rather than along the mathematical

surface, but it is worth noting that each streamline does define a form of shortest distance. Recall also that measuring width along the shortest distance on the spherical earth is the shortest-path definition of width, which lacks the uniqueness property featured by the streamline definition as illustrated in section 2.

It should be recognized that other definitions of MIZ width may be more useful in operational settings where the context may be pragmatic rather than scientific. For example, the captain of a vessel is not likely to follow a streamline through the MIZ unless there is reason to traverse along the gradient of the (idealized) concentration field. The width in such an operational context might instead be more usefully defined as the shortest distance across the MIZ. In the absence of extreme curvature, though, note that the shortest-distance and streamline definitions are not markedly different (e.g., consider the streamlines in Figs. 2c,d). Local streamline-based MIZ widths may thus provide a useful overlay for operational resources such as the National Ice Center's MIZ product (NIC 2016), especially for reasonably behaved MIZ geometries.

The MIZ continues to be the focus of innovative modeling and intensive field campaigns such as the Marginal Ice Zone Program (Lee et al. 2012), and much has been learned about, for example, the role of melt ponds in the summer breakup of Arctic sea ice cover (Arntsen et al. 2015), the role of lateral melting in the seasonal evolution of sea ice floe size distribution (Perovich and Jones 2014; Zhang et al. 2015), and the potential for sea ice prediction on seasonal time scales (Lindsay et al. 2012; Steele et al. 2015). Considering directions for continued research on MIZ width, Stroeve et al. (2016) analyzed MIZ trends for the Antarctic in all months except summer, when signal-to-noise ratios decline, and Strong and Rigor (2013) found a 39% widening of the warm-season Arctic MIZ with much smaller narrowing of the cold-season Arctic MIZ. Comparatively little has been reported on long-term change and variability in MIZ width during the Arctic transition seasons. Also, the approximately 40% widening of the Arctic warm-season MIZ may motivate modeling–observational analyses to understand the roles of thermodynamic versus dynamic, and oceanic versus atmospheric drivers of these changes.

Acknowledgments. We gratefully acknowledge the support from the Division of Mathematical Sciences at the U.S. National Science Foundation (NSF) through Grants DMS-1413454 and DMS-0940249. We are also grateful for the support from the Arctic and Global Prediction Program at the Office of Naval Research (ONR) through Grant N00014-13-10291, and we thank the NSF Mathematics and Climate Research Network (MCRN) for its support of this work. Finally, we thank two anonymous reviewers for comments that helped to improve an earlier draft of the manuscript.

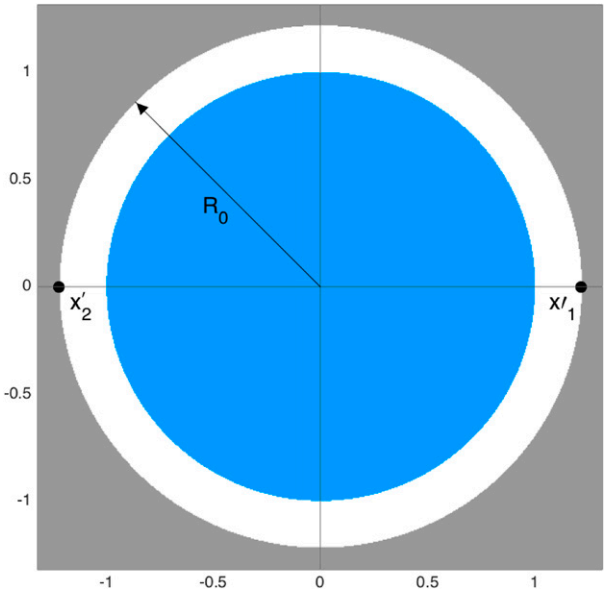

FIG. A1. Conformal mapping of the eccentric annulus from the z plane in Fig. 4a to the w plane.

APPENDIX A

Solution to Laplace's Equation

We consider an annulus Ω (shown in white in Fig. 4) on the z plane. Its outer circle centered at the origin is scaled to have a unit radius $r_2 = 1$. This represents the outer boundary of the MIZ at the marginal ice–ocean interface, where sea ice concentration $\phi = 0.15$. Its inner circle with radius r_1 is centered at $x_0 \in (r_1 - 1, 1 - r_1)$ and represents the inner boundary of the MIZ at the marginal ice–inner pack ice interface, where $\phi = 0.80$. Domain Ω is mapped to the area between concentric circles in the w plane (Fig. A1) via the linear fractional transformation (e.g., Brown and Churchill 2009)

$$w = \frac{z - a}{az - 1}, \tag{A1}$$

where a is given by

$$a = \frac{1 + x_1 x_2 + [(1 - x_1^2)(1 - x_2^2)]^{1/2}}{x_1 + x_2}. \tag{A2}$$

The inner circle on the z plane is mapped to a circle on the w plane with the center at the origin and radius

$$R_0 = \frac{1 - x_1 x_2 + [(1 - x_1^2)(1 - x_2^2)]^{1/2}}{x_1 - x_2}. \quad \text{(A3)}$$

On the w plane, Laplace's equation $\nabla^2\Phi = 0$ has a solution given by the complex potential

$$F(w) = \alpha \ln w + k, \quad \text{(A4)}$$

which has a real part $\phi = \alpha \ln|w| + k$ called the potential and an imaginary part $\psi = \alpha \arg w$ called the streamfunction. Boundary conditions $\phi(|w| = R_0) = 0.80$ and $\phi(|w| = 1) = 0.15$ yield $k = 0.15$ and $\alpha = (0.80 - 0.15)/\ln R_0$. Functions ϕ and ψ on the z plane are given by

$$\phi = \alpha \ln\left|\frac{z - a}{az - 1}\right| + k, \quad \text{(A5)}$$

$$\psi = \alpha \arg\left(\frac{z - a}{az - 1}\right), \quad \text{(A6)}$$

respectively. The width ℓ of the annulus Ω at any point can be defined as the arc length of the level set of ψ through that point on the z plane. On the w plane, the level set $\{w \in \mathbb{C}: \psi = \psi_c\}$ is the parametric line

$$w(t) = t \exp(i\psi_c/\alpha); \quad 1 \le t \le R_0, \quad \text{(A7)}$$

which is mapped to the z plane as

$$z(t) = \frac{t \exp(i\psi_c/\alpha) - a}{a\, t \exp(i\psi_c/\alpha) - 1}; \quad 1 \le t \le R_0. \quad \text{(A8)}$$

The modulus of the derivative in Eq. (A8) is given by

$$|z'(t)| = \frac{a^2 - 1}{a^2 t^2 - 2at\cos(\psi_c/\alpha) + 1}, \quad \text{(A9)}$$

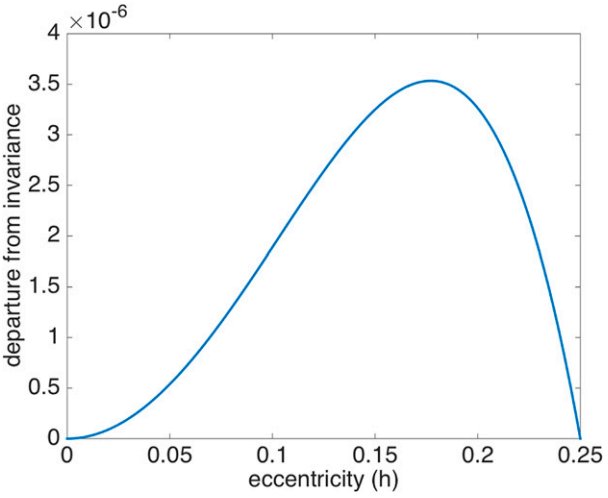

FIG. B1. Departure of $\bar{\ell}_*$ from invariance [i.e., $\bar{\ell}_* - (r_2 - r_1)$] as a function of eccentricity (h).

and so for the arc length

$$\ell := \int_1^{R_0} |z'(t)|\, dt \quad \text{(A10)}$$

we have Eq. (4) in the main text.

APPENDIX B

Existence and Uniqueness of ϕ_*

We consider function (4) and introduce a variable $\tau = \psi_c/\alpha$ in the same domain. Using the arctangent addition property, we rewrite $\ell(\tau)$ as

$$\ell(\tau) = \begin{cases} \dfrac{a^2 - 1}{a\sin(\tau)} \tan^{-1} \dfrac{a(R_0 - 1)\sin(\tau)}{1 + a^2 R_0 - a(1 + R_0)\cos(\tau)} & \text{if } \tau \notin \{0, \pi\} \\ 1 + x_2 & \text{if } \tau = 0 \\ 1 - x_1 & \text{if } \tau = \pi \end{cases}. \quad \text{(B1)}$$

This function will be considered on the restricted domain $\tau \in [0, \pi]$, as the objects studied in this case are symmetric with regard to the top and bottom halves of the annular domain. To show that for a given specific length the appropriate level set of ψ exists and is unique, we will show that the function $\ell(\tau)$ is continuous and monotonic and hence possesses the intermediate value property.

First, we notice that the function $\ell(\tau)$ in Eq. (B1) is continuous on the interval $0 < \tau < \pi$ as a composition of continuous functions. Therefore, the only points where the continuity of $\ell(\tau)$ comes into question is at the endpoints, 0 and π. To check the behavior of the function at these points, we calculate the limits of $\ell(\tau)$ when τ goes to zero and to π using L'Hôpital's rule, as both limits are indeterminate. Using expressions for a and R_0

[Eqs. (A2) and (A3), respectively] and with some algebra we obtain

$$\lim_{\tau\to 0^+}\ell(\tau)=\frac{(a+1)(R_0-1)}{aR_0-1}=1+x_2,$$

$$\lim_{\tau\to \pi^-}\ell(\tau)=\frac{(a-1)(R_0-1)}{aR_0+1}=1-x_1.$$

Because the limits match the definition of $\ell(\tau)$ in Eq. (B1), we conclude that this function is continuous.

Now we show that the function $\ell(\tau)$ in Eq. (B1) is monotonic. To show this, we make some observations. First, note that we are specifically referring to the monotonicity with respect to the variable τ and only on the domain mentioned earlier. Let us split this domain into two halves. First, consider the behavior of the function on the interval $[0, \pi/2]$. The denominator of $\ell(\tau)$ is increasing while the argument of the arctangent is decreasing. These effects combine to produce a net monotonic decrease in the interval. On the second half, from $[\pi/2, \pi]$, the arctangent term tends to zero much faster than the denominator as a result of the combined effects of its interior composition. One can check that the derivative at $\tau=\pi/2$ is $\{-a(a^2-1)(R_0^2-1)/[(1+a^2R_0)^2+a^2(R_0-1)^2]\}$. The function exhibits monotonically decreasing behavior as it limits toward $1-x_1$.

From these analytic results, we glean several useful pieces of information. First, since the function (B1) is continuous, it has the intermediate value property. This translates to the fact that every length between $1+x_2$ to $1-x_1$ exists and has a corresponding value of ψ. The fact that Eq. (B1) is monotonic also means that the each unique length has a unique value of ψ. There exists no two streamfunctions, ψ, that have the same length on $(0, \pi)$. Finally, since the potential function (2) is harmonic, $\bar{\ell}_{\phi_*}$ inherits both of these properties. Continuity is preserved by the integration, and monotonicity is preserved by the positive nature of the function (B1).

REFERENCES

Arntsen, A. E., A. J. Song, D. K. Perovich, and J. A. Richter-Menge, 2015: Observations of the summer breakup of an Arctic sea ice cover. *Geophys. Res. Lett.*, **42**, 8057–8063, doi:10.1002/2015GL065224.

Barber, D. G., and Coauthors, 2015: Selected physical, biological and biogeochemical implications of a rapidly changing Arctic Marginal Ice Zone. *Prog. Oceanogr.*, **139**, 122–150, doi:10.5194/tc-6-881-2012.

Brown, J. W., and R. V. Churchill, 2009: *Complex Variables and Applications.* McGraw-Hill, 468 pp.

Cavalieri, D. J., and C. L. Parkinson, 2012: Arctic sea ice variability and trends, 1979–2010. *Cryosphere*, **6**, 881–889, doi:10.5194/tcd-6-957-2012.

Comiso, J. C., 2006: Abrupt decline in Arctic winter sea ice cover. *Geophys. Res. Lett.*, **33**, L18504, doi:10.1029/2006GL027341.

——, 2012: Large decadal decline of the Arctic multiyear ice cover. *J. Climate*, **25**, 1176–1193, doi:10.1175/JCLI-D-11-00113.1.

——, and H. J. Zwally, 1984: Concentration gradients and growth/decay characteristics of the seasonal sea ice cover. *J. Geophys. Res.*, **89**, 8081–8103, doi:10.1029/JC089iC05p08081.

Glendening, J. W., 1994: Dependence of boundary layer structure near an ice-edge coastal front upon geostrophic wind direction. *J. Geophys. Res.*, **99**, 5569–5581, doi:10.1029/93JD02925.

Jones, S. E., B. R. Buchbinder, and I. Aharon, 2000: Three-dimensional mapping of cortical thickness using Laplace's equation. *Hum. Brain Mapp.*, **11**, 12–32, doi:10.1002/1097-0193(200009)11:1<12::AID-HBM20>3.0.CO;2-K.

Lagarias, J., J. A. Reeds, M. H. Wright, and P. E. Wright, 1998: Convergence properties of the Nelder–Mead simplex method in low dimensions. *SIAM J. Optim.*, **9**, 112–147, doi:10.1137/S1052623496303470.

Lee, C. M., and Coauthors, 2012: Marginal Ice Zone (MIZ) Program: Science and experiment plan. Applied Physics Laboratory, University of Washington, Tech. Rep. APL-UW 1201, 48 pp.

Lindsay, R., and Coauthors, 2012: Seasonal forecasts of Arctic sea ice initialized with observations of ice thickness. *Geophys. Res. Lett.*, **39**, L21502, doi:10.1029/2012GL053576.

Livina, V. N., and T. M. Lenton, 2013: A recent tipping point in the Arctic sea-ice cover: Abrupt and persistent increase in the seasonal cycle since 2007. *Cryosphere*, **7**, 275–286, doi:10.5194/tc-7-275-2013.

Meier, W., F. Fetterer, M. Savoie, S. Mallory, R. Duerr, and J. Stroeve, 2012: NOAA/NSIDC Climate Data Record of Passive Microwave Sea Ice Concentration, version 2 (updated 2016). National Snow and Ice Data Center, accessed 11 November 2016, doi:10.7265/N55M63M1.

NIC, 2016: Products. Naval Ice Center. [Available online at http://www.natice.noaa.gov/Main_Products.htm.]

Perovich, D. K., and K. F. Jones, 2014: The seasonal evolution of sea ice floe size distribution. *J. Geophys. Res. Oceans*, **119**, 8767–8777, doi:10.1002/2014JC010136.

Perrette, M., A. Yool, G. D. Quartly, and E. E. Popova, 2010: Near-ubiquity of ice-edge blooms in the Arctic. *Biogeosciences*, **8**, 515–524, doi:10.5194/bg-8-515-2011.

Polyakov, I. V., J. E. Walsh, and R. Kwok, 2012: Recent changes of Arctic multiyear sea ice coverage and the likely causes. *Bull. Amer. Meteor. Soc.*, **93**, 145–151, doi:10.1175/BAMS-D-11-00070.1.

Post, E., and Coauthors, 2013: Ecological consequences of sea-ice decline. *Science*, **341**, 519–524, doi:10.1126/science.1235225.

Ribic, C. A., D. G. Ainley, and W. Fraser, 1991: Habitat selection by marine mammals in the marginal ice zone. *Antarct. Sci.*, **3**, 181–186, doi:10.1017/S0954102091000214.

Rogers, T. S., J. E. Walsh, T. S. Rupp, L. W. Brigham, and M. Sfraga, 2013: Future Arctic marine access: Analysis and evaluation of observations, models, and projections of sea ice. *Cryosphere*, **7**, 321–332, doi:10.5194/tc-7-321-2013.

Schmale, J., M. Lisowska, and M. Smieszek, 2013: Future Arctic research: Integrative approaches to scientific and methodological challenges. *Eos, Trans. Amer. Geophys. Union*, **94**, 292–292, doi:10.1002/2013EO330004.

Shaw, W. J., R. L. Pauley, T. M. Gobel, and L. F. Radke, 1991: A case study of atmospheric boundary layer mean structure for flow parallel to the ice edge: Aircraft observations from

CEAREX. *J. Geophys. Res.*, **96**, 4691–4708, doi:10.1029/90JC01953.

Squire, V. A., 1998: The marginal ice zone. *Physics of Ice-covered Seas*, M. Lepparanta, Ed., Vol. 1, Helsinki University Printing House, 381–446.

——, 2007: Of ocean waves and sea-ice revisited. *Cold Reg. Sci. Technol.*, **49**, 110–133, doi:10.1016/j.coldregions.2007.04.007.

Stammerjohn, S., R. Massom, D. Rind, and D. Martinson, 2012: Regions of rapid sea ice change: An inter-hemispheric seasonal comparison. *Geophys. Res. Lett.*, **39**, L06501, doi:10.1029/2012GL050874.

Steele, M., S. Dickinson, J. Zhang, and R. W. Lindsay, 2015: Seasonal ice loss in the Beaufort Sea: Toward synchrony and prediction. *J. Geophys. Res. Oceans*, **120**, 1118–1132, doi:10.1002/2014JC010247.

Stephenson, S. R., L. C. Smith, and J. A. Agnew, 2011: Divergent long-term trajectories of human access to the Arctic. *Nat. Climate Change*, **1**, 156–160, doi:10.1038/nclimate1120.

Stroeve, J. C., S. Jenouvrier, G. G. Campbell, C. Barbraud, and K. Delord, 2016: Mapping and assessing variability in the Antarctic marginal ice zone, pack ice and coastal polynyas in two sea ice algorithms with implications on breeding success of snow petrels. *Cryosphere*, **10**, 1823–1843, doi:10.5194/tc-10-1823-2016.

Strong, C., 2012: Atmospheric influence on Arctic marginal ice zone position and width in the Atlantic sector, February–April 1979–2010. *Climate Dyn.*, **39**, 3091–3102, doi:10.1007/s00382-012-1356-6.

——, and I. G. Rigor, 2013: Arctic marginal ice zone trending wider in summer and narrower in winter. *Geophys. Res. Lett.*, **40**, 4864–4868, doi:10.1002/grl.50928.

Thomson, J., and W. E. Rogers, 2014: Swell and sea in the emerging Arctic Ocean. *Geophys. Res. Lett.*, **41**, 3136–3140, doi:10.1002/2014GL059983.

Tilling, R. L., A. Ridout, A. Shepherd, and D. J. Wingham, 2015: Increased Arctic sea ice volume after anomalously low melting in 2013. *Nat. Geosci.*, **8**, 643–646, doi:10.1038/ngeo2489.

Wadhams, P., 2000: *Ice in the Ocean*. Gordon and Breach Science Publishers, 351 pp.

Weeks, W. F., 2010: *On Sea Ice*. University of Alaska Press, 664 pp.

Williams, R., and Coauthors, 2014: Counting whales in a challenging, changing environment. *Sci. Rep.*, **4**, 4170, doi:10.1038/srep04170.

Williams, T. D., L. G. Bennetts, V. A. Squire, D. Dumont, and L. Bertino, 2013: Wave–ice interactions in the marginal ice zone. Part 2: Numerical implementation and sensitivity studies along 1D transects of the ocean surfaces. *Ocean Modell.*, **71**, 92–101, doi:10.1016/j.ocemod.2013.05.011.

WMO, 2009: WMO sea-ice nomenclature. WMO/OMM/BMO 259, Suppl. 5, 23 pp. [Available online at http://www.jcomm.info/index.php?option=com_oe&task=viewDocumentRecord&docID=4438.]

Zang, J., A. Schweiger, M. Steele, and H. Stern, 2015: Sea ice floe size distribution in the marginal ice zone: Theory and numerical experiments. *J. Geophys. Res. Oceans*, **120**, 3484–3498, doi:10.1002/2015JC010770.